Free-Flight and Wind-Tunnel Data for a Generic Fighter Configuration

G.L. Winchenbach*
Eglin Air Force Base, Florida
R. L. Uselton†
Calspan Field Services, Arnold Airforce Station, Tennessee
W. H. Hathaway‡
General Electric Company, Burlington, Vermont
and
R. M. Chelekis§
Air Force Armament Laboratory, Eglin Air Force Base, Florida

A comparison of free-flight spark range and wind-tunnel data for a generic fighter configuration (standard dynamics model) is presented. The aerodynamic tests were conducted from 0.3 to 1.3 with the primary comparisons at the transonic Mach numbers. This paper shows the comparison of the zero angle-of-attack coefficients and derivatives since only relatively small oscillation amplitudes were achieved during the free-flight tests. However, it is believed that this comparison represents good agreement between these two sets of data obtained in different facilities using different test mechanisms and techniques.

Nomenclature

b = wing span
CG = center of gravity
CG_R = reference center of gravity
C_l = roll moment coefficient, l/QSb
C_{lp} = slope of the roll moment vs spin
$C_{l\beta}$ = slope of the roll moment vs β
$C_{l\gamma\alpha 2}$ = induced roll moment coefficient
$C_{l\delta}$ = slope of the roll moment vs fin cant
C_m = pitching moment coefficient, pitch moment/$QS\bar{c}$
C_{m0}, C_{n0} = zero angle pitch and yaw moment coefficients
C_{mq} = pitch damping coefficient,

$$\frac{\partial C_m}{\partial}\frac{q_b(\bar{c})}{2V}+\frac{\partial C_m}{\partial}\frac{\dot{\alpha}(\bar{c})}{2V}$$

C_{mq2}, C_{nr2} = quadratic pitch damping and quadratic yaw damping coefficients
$C_{m\gamma\alpha}$ = slope of pitching moment vs α
$C_{m\alpha 2}$, $C_{n\beta 2}$ = quadratic pitching and yawing moment coefficients
$C_{m\alpha 3}$, $C_{n\beta 3}$ = cubic pitching and yawing moment coefficients
$C_{m\gamma\alpha 3}$, $C_{n\gamma\alpha 3}$ = roll induced pitching and yawing moment coefficients
C_n = yawing moment coefficients, side moment/QSb)
C_{nr} = yaw damping coefficient,

$$\frac{\partial C_n}{\partial}\frac{r_b b}{2V}-\frac{\partial C_n}{\partial}\frac{\dot{\beta} b}{2V}$$

$C_{n\beta}$ = slope of yawing moment vs β
C_x = axial force coefficient, axial force/QS
C_{x0} = axial force coefficient at zero angle of attack
C_{xm} = slope of axial force coefficient vs Mach
$C_{x\alpha}$ = slope of axial force coefficient vs α
$C_{x\alpha 2}$, $C_{x\beta 2}$ = quadratic axial force coefficients
C_y = side force coefficient, side force/QS
C_{y0}, C_{z0} = zero angle side and normal force
$C_{y\beta}$ = slope of the side force vs β
$C_{y\beta 2}$, $C_{z\alpha 2}$ = quadratic side and normal force coefficients
$C_{y\beta 3}$, $C_{z\alpha 3}$ = cubic side and normal force coefficients
$C_{y\gamma\alpha 3}$, $C_{a\gamma\alpha 3}$ = roll induced side and normal force coefficients
C_z = normal force coefficient, normal force/QA
$C_{z\alpha}$ = slope of the normal force vs α
D, d = model base diameter
d_s = diameter of sting at model base
I_x, I_y, I_z = moments of inertia about the X, Y, and Z axis
l = model length
l_s = effective sting length (model base to start of flare)
M = Mach number
MAC, ($\bar{c}$) = mean aerodynamic cord of the wing
M_R = reference Mach number
N = number of the planes of symmetry
P_b, q_b, r_b = rolling, pitching, and yawing velocities
PT = tunnel stilling chamber pressure
Q = dynamic pressure
Re = wind-tunnel freestream Reynolds number, ft^{-1}
$R_{e\bar{c}}$ = freestream Reynolds number based on MAC
S = reference area, wing plan form area (includes fuselage section)
TT = tunnel stilling chamber temperature

Presented as Paper 82-1365 at the 9th Atmospheric Flight Mechanics Conference, San Diego, Calif., Aug. 9-11, 1982; received Oct. 14, 1982; revision received June 27, 1983. This paper is declared a work of the U.S. Government and therefore is in the public domain.

*Section Chief, Exterior Ballistics, Direct Fire Weapons Division. Member AIAA.
†Supervisor, Dynamic Stability Section, Von Karman Facility, AEDC Division. Member AIAA.
‡Advanced Design Engineer, Armament and Electrical Systems Department. Member AIAA.
§Lieutenant, Project Engineer, Direct Fire Weapons Division.

u_b, v_b, w_b = body fixed velocities in the X, Y, Z directions
V = total velocity (or, freestream velocity in tunnel)
x,y,z = fixed plane coordinates
α, β = pitch and yaw angles, angle of attack, angle of side slip
$\bar{\alpha}$ = total angle of attack
$\bar{\alpha}_M$ = maximum total angle of attack
γ = aerodynamic roll angle
δ = wing, tail misalignment
ξ = sine of the total angle of attack, $[(V_b^2 + w_b^2)/v^2]^{1/2}$
ω = oscillation frequency

Superscripts

$\dot{(\ )}$ = first derivative with respect to time
$\bar{(\ )}$ = total values

Subscripts

$\bar{\alpha}$ = derivative with respect to ξ_i
$\bar{\alpha}_i$ = derivative with respect to ξ
α = derivative with respect to α
β = derivative with respect to β
γ = derivative with respect to γ

Introduction

THE overall purpose of the present range and wind-tunnel experiments was to increase the static and dynamic aerodynamic coefficient data base associated with a generic fighter configuration. This configuration, the standard dynamics model (SDM), has been or will be tested in various free world facilities. This accumulated data base will be used to improve aerodynamic prediction routines for future advanced aircraft.

An additional objective of the free-flight spark range tests was to obtain interference free aerodynamic data at transonic Mach numbers which could be used to assess possible tunnel interference effects. The purpose of this paper is not to discuss interference effects, per se, but to compare the aerodynamic data as obtained from a free-flight spark range with that obtained from wind tunnel. It is believed that this comparison is significant since very little free-flight spark range data for an aircraft configuration are available and even less have been compared with wind-tunnel data for the same configuration and at similar test conditions.

Facilities, Models, and Test Conditions

Free-Flight Range

The free-flight tests[1] were conducted in the Aeroballistic Research Facility (ARF)[2] which is part of the Ballistics Branch, Direct Fire Weapons Division, Air Force Armament Laboratory, Eglin Air Force Base, Florida. This facility is an enclosed, atmospheric, instrumented, concrete structure used to examine the exterior ballistics of various free-flight configurations. The facility contains a gun room, control room, model measurements room, blast chamber, and the instrumented range.

The 207-m instrumented length of the range has a 3.6-m^2 cross section for the first 69 m and a 4.88-m^2 cross section for the remaining length. The range has 131 locations available as instrumentation sites. Each location has a physical separation of 1.52 m, and presently 50 of the sites are used to house fully instrumented orthogonal shadowgraph stations. The maximum shadowgraph window, an imaginery circle in which a projectile in flight will cast a shadow on both reflected screen, is 2.13 m in diameter. A laser-lighted photographic station is located in the uprange end of the instrumented range. This photographic station yields four orthogonal photographs, permitting a complete 360-deg view of the projectile as it passes the station on its downrange trajectory. Also, a direct shadowgraph station, consisting of a spark gap and film holder, is located in the uprange end of the range. Since the film is illuminated directly by the spark as the model passes the station, high-quality flow photographs are obtained. The nominal operating temperature of the range is 22°C.

Wind Tunnels

The dynamic stability wind-tunnel tests[3,4] were performed in the Aerodynamic Wind Tunnel (4T), in the Propulsion Wind Tunnel Facility (PWT), Arnold Engineering Development Center (AEDC), Arnold Air Force Station, Tennessee. Aerodynamic Wind Tunnel (4T) is a closed-loop, continuous flow, variable-density tunnel in which the Mach number can be varied from 0.1 to 1.3 and can be set at discrete Mach numbers of 1.6 and 2.0 by placing nozzle inserts over the permanent sonic nozzle. At all Mach numbers, the stagnation pressure can be varied from 400 to 3400 psfa. The test section is 4 ft^2 and 12.5-ft long with perforated, variable porosity walls. The model support system consists of a sector and boom attachment which has a pitch angle capability of −7.5-28 deg about the sting centerline.

The forced oscillation test mechanism used for the pitch/yaw damping tests[3] utilizes a cross-flexure pivot, an electric shaker motor, and a one-component moment beam which is instrumented with strain gages to measure the forcing moment of the shaker motor. The electric motor is coupled to the moment beam by means of a connecting rod and a flexural linkage which converts the translational force to a moment to oscillate the model at amplitudes up to 3 deg and frequencies from 2 to 8 Hz. Data for the present tests were obtained with the 0.180-in.-thick cross flexures, having a stiffness of 962.5 ft-lb/rad. The moment beam used to measure the pitch-damping moments has a thickness of 0.047 in. and is capable of measuring a total moment of 11.3 in.-lb. For measuring the yaw-damping moments, the moment beam thickness was 0.035 in., which is capable of measuring a total moment of 7.1 in.-lb. Effective sting length ratio (l_s/d) and sting diameter ratio (d_s/d) for the pitch/yaw damping tests were 5.7 and 0.4, respectively.

The test mechanism used for the roll-damping tests consisted of a cross-flexure pivot connected to a hydraulic cylinder through a force-measuring flexure. The hydraulic cylinder is operated with a servo valve to obtain sinusoidal oscillation motion at a constant oscillation amplitude, up to ±2 deg, and constant frequency from 2 to about 10 Hz. The cross flexure is instrumented to measure angular displacement, also, supports model loads and provides the restoring moment to cancel the inertia moment when the system is operating at the natural frequency of the model/balance assembly. The restoring moment for the roll mechanism was 43 in.-lb/deg. For the roll damping tests, l_s/d was 6.8 and d_s/d was 0.45.

Both mechanisms utilized control and readout systems for setting the oscillation frequency and amplitude. An electronic position feedback loop is used to maintain a constant oscillation amplitude and frequency under aerodynamic loads and permits testing both dynamically stable and unstable configurations. Data are normally obtained at the natural frequency of the model/flexure spring-mass system.

The static force and moment data are documented in Ref. 3. These data were also obtained in Aerodynamic Wind Tunnel (4T) utilizing a standard static force balance. The static force data were obtained utilizing a sting with an effective sting length ratio (l_s/d) of 8.9 and a sting diameter ratio (d_s/d) of 0.41.

Models for Test Conditions

The free-flight SDM represents a 1/72 scale generic fighter (Fig. 1). The desired center of gravity for the flight models [approximately 15% of the mean aerodynamic chord, (MAC)] was obtained using a brass nose section. Table 1

Table 1 Physical properties of free flight models

Shot No.	MAC, cm	Mass, g	I_x, g-cm^2	I_y, g-cm^2	I_z, g-cm^2	CG, % MAC	Length, cm	CG, % l	CG, cm, Fram Nose
S80121057	4.7422	288.00	517.470	7847.9	8120.0	15.39	19.424	0.5365	10.421
S80121258	4.7422	288.78	520.860	7846.8	8142.8	15.42	19.419	0.5366	10.420
S80121559	4.7422	287.28	515.211	7868.3	8104.4	15.12	19.455	0.5358	10.424
S81020560	4.7422	273.95	485.835	7551.0	7737.2	14.02	19.570	0.5329	10.429
S81020661	4.7422	271.89	486.174	7429.7	7655.6	15.10	19.528	0.5356	10.459
S81021063	4.7422	274.90	474.988	7505.0	7720.0	14.50	19.507	0.5342	10.421
S81021164	4.7422	273.02	488.659	7453.6	7673.9	14.59	19.503	0.5344	10.422
S81021968	4.7422	276.70	482.445	7590.3	7751.9	14.54	19.496	0.5343	10.417
S81031171	4.7422	276.14	509.222	7488.9	7696.0	13.68	19.504	0.5322	10.380
S81031372	4.7422	278.42	508.206	7635.3	7843.2	13.43	19.613	0.5314	10.422
S81031373	4.7422	277.51	499.280	7556.8	7755.4	13.48	19.514	0.5317	10.376
S81031674	4.7422	275.10	505.155	7409.1	7616.2	13.89	19.458	0.5328	10.368
S81032575	4.7422	273.52	503.573	7418.6	7622.0	15.10	19.477	0.5357	10.434
S81032676	4.7422	274.37	504.703	7471.7	7670.5	14.75	19.510	0.5348	10.434
S81032677	4.7422	273.07	503.347	7248.8	7636.6	14.74	19.491	0.5348	10.424
S81032799	4.7422	276.14	505.042	7468.9	7658.1	14.94	19.485	0.5353	10.431
S81040881	4.7422	276.51	507.302	7531.6	7720.3	14.29	19.490	0.5337	10.402
S81040882	4.7422	274.68	505.042	7458.1	7649.1	14.62	19.491	0.5345	10.418
S81040883	4.7422	277.44	505.720	7543.1	7753.0	13.66	19.477	0.5322	10.366

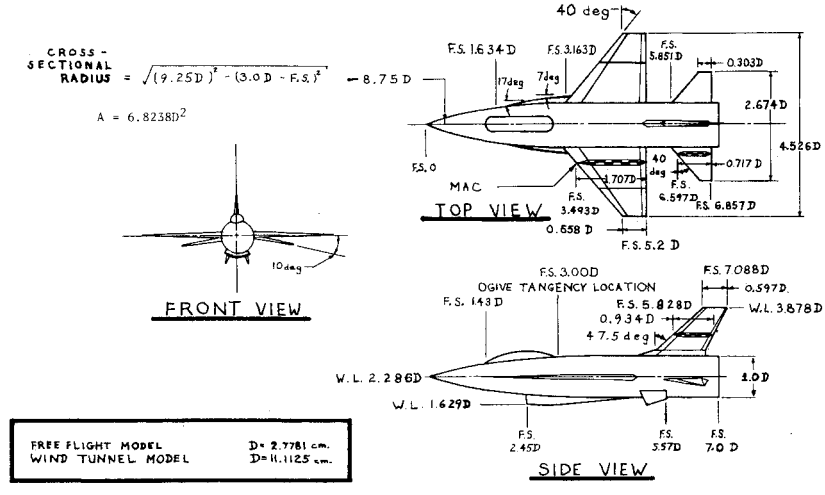

Fig. 1 Standard dynamics model (SDM) details

presents the mass properties of the free flight models. The sabots used for the free-flight tests were of a four segment design as shown in Fig. 2. The wind-tunnel model designed and fabricated at AEDC was four times larger than the free-flight models and was tested at two different center-of-gravity locations of 15% and 35% of the MAC. The data comparisons in this paper are for the 15% center-of-gravity location only. All external components (i.e., wings, stabilizers, inlet, ventral fins, canopy) of the wind-tunnel model may be removed for buildup testing as desired.

All the flight models were launched at atmospheric pressure conditions and at Mach numbers between 0.6 and 1.15. The wind-tunnel tests were conducted at Mach numbers of 0.3-1.3. A list of the free-flight test conditions is shown in Table 2 and the wind-tunnel test conditions are shown in Table 3. A typical flowfield photograph of a model in free flight is shown in Fig. 3a, and a photograph of the SDM installed in the wind tunnel is shown in Fig. 3b.

Free-Flight Data Reduction

The primary goal in analyzing the experimental trajectories is to determine the aerodynamic forces and moments acting on the SDM model during the observed motions (range flights). This requires fitting the six degree of freedom dynamic data acquired from the spark range to the equations of motion assumed to characterize that flight. The resultant fit accuracy should be approximately equivalent to the data measurement capability of the range if the aerodynamic model is functionally adequate. In general, the aerodynamics are nonlinear functions of the angle of attack, Mach number, and aerodynamic roll angle.

The data analysis system currently in use for extracting the aerodynamic coefficients and derivatives from the trajectories measured in the ARF is shown in Fig. 4.[5,6] This system incorporates a standard linear theory analysis and coupled six degree of freedom (6DOF) analysis. The 6DOF routines incorporate the maximum likelihood method (MLM) data correlation technique to match the theoretical trajectories to that measured experimentally. As used in the present routines, the MLM is an iterative procedure which adjusts the aerodynamic coefficients to maximize a likelihood function providing a best fit to the data.

This data reduction system correlates the 6DOF equations of motion, containing the nonlinear aerodynamic model, directly to the measured motion. Also, multiple data sets (up to five) can be simultaneously fit to a common set of aerodynamics. Using this multiple fit approach, a more complete range of angle of attack and roll orientation combinations are available for analysis than would be available from any one particular flight considered separately. This increases the accuracy of the determined aerodynamics over the entire range of angles of attack and roll combinations.

ARFDAS, Fig. 4, represents a complete ballistic range data reduction system capable of analyzing both symmetric and

unsymmetric bodies. The essential steps of the data reduction system are to 1) assemble the basic dynamic range data (time vs x, y, z, θ, ψ, ϕ), physical properties, and atmospheric conditions; 2) perform linear theory analysis; and 3) perform 6DOF analysis. These steps have been integrated into ARFDAS to provide the test engineer with a convenient and efficient means of interaction. At each step into the analysis, permanent records for each shot are maintained by ARFDAS such that subsequent analyses with data modifications are much faster.

The aerodynamic data presented in this paper were obtained using the body-fixed 6DOF analysis (MLMBDFX) with the multiple fit data correlation technique. The equations of motion are derived with respect to a rotating coordinate system. This coordinate system is defined with the x axis aligned with the longitudinal axis of the model and points out the nose; the y axis points out the left wing; and the z axis points up with respect to the body. The body-fixed coordinate system is rigidly attached to the model and rotates with the model about its x axis. The equations of motion and aerodynamic force and moment definitions are described and discussed in Refs. 5 and 6. These were unchanged for the SDM reductions and will not be elaboratored on herein. However, the generalized aerodynamic coefficient expansions were modified for the SDM reductions and are defined as follows.

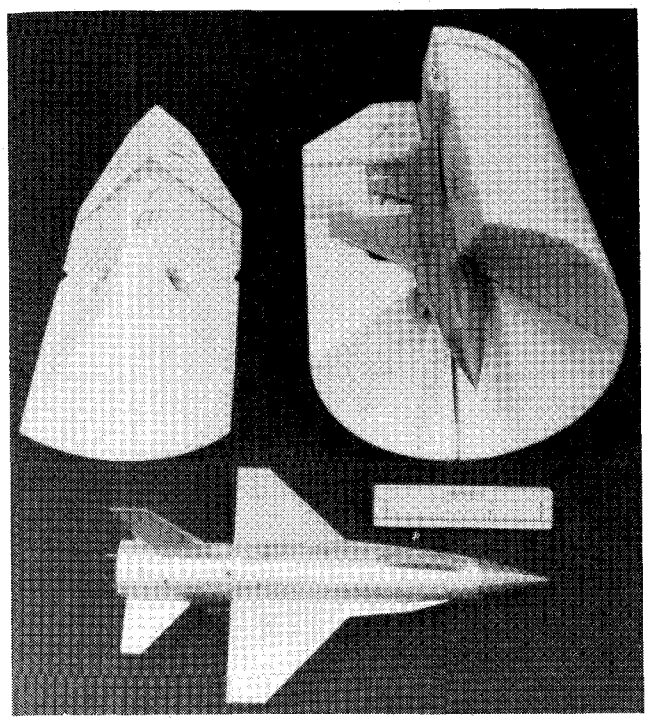

Fig. 2 Model sabot photograph

$$\bar{C}_x = C_{x0} + C_{x\alpha}(W_b/V) + C_{x\alpha 2}(w_b/V)^2 + C_{x\beta 2}(v_b/V)^2 + C_{xm}(M - M_R) \quad (1)$$

$$\bar{C}_{Y0} = C_{Y0} \quad (2)$$

$$\bar{C}_{z0} = C_{z0} \quad (3)$$

$$\bar{C}_{Y\beta} = C_{Y\beta} + C_{Y\beta 3}(v_b/V)^2 + C_{Y\gamma\bar{\alpha}3}\xi^2\cos(N\gamma) \quad (4)$$

$$\bar{C}_{z\alpha} = C_{z\alpha} + C_{z\alpha 2}(w_b/V) + C_{z\alpha 3}(w_b/V)^2 + C_{z\gamma\bar{\alpha}3}\xi^2\cos(N\gamma) \quad (5)$$

$$\bar{C}_{Y\gamma\alpha} = C_{Y\gamma\bar{\alpha}3}\xi^2\sin(N\gamma) \quad (6)$$

$$\bar{C}_{Yp\alpha} = C_{Yp\alpha} \quad (7)$$

$$\bar{C}_{lp} = C_{lp} \quad (8)$$

$$\bar{C}_l = C_{l\delta}\delta + C_{l\gamma\bar{\alpha}}\xi^2\sin(N\gamma) + C_{l\beta}(v_b/V) \quad (9)$$

$$\bar{C}_{m0} = C_{m0} \quad (10)$$

$$\bar{C}_{n0} = C_{n0} \quad (11)$$

$$\bar{C}_{m\alpha} = C_{m\alpha} + C_{m\alpha 2}(v_b/V) + C_{m\alpha 3}(v_b/V)^2 + C_{m\gamma\bar{\alpha}3}\xi^2\cos(N\gamma) + C_{z\alpha}(CG - CG_R) \quad (12)$$

$$\bar{C}_{mq} = C_{mq} + C_{mq\alpha 2}(w_b/V)^2 \quad (13)$$

$$\bar{C}_{n\beta} = C_{n\beta} + C_{n\beta 3}(v_b/V)^2 + C_{n\gamma\bar{\alpha}3}\xi^2\cos(N\gamma) + C_{Y\beta}(CG - CG_R) \quad (14)$$

$$\bar{C}_{nr} = C_{nr} + C_{nr\beta 2}(v_b/V)^2 \quad (15)$$

$$\bar{C}_{n\gamma\alpha} = C_{n\gamma\bar{\alpha}3}\xi^2\sin(N\gamma) \quad (16)$$

Table 2 Free-flight test conditions

Shot No.	No. of stations	Observed Distance (M)	Air density, g/cm^2	Speed of sound, m/s	$Re_{\bar{c}} \times 10^{-6}$	Mach No.
S80121057	11	39.6	0.0012031	343.85	0.855	0.779
S80121258	17	54.8	0.0012099	344.43	1.226	1.111
S80121559	13	51.7	0.0011967	344.43	0.683	0.624
S80120560	18	79.0	0.0012151	344.43	1.215	1.087
S81020661	19	76.1	0.0012024	345.01	0.853	0.774
S81021063	21	82.3	0.0011856	344.72	0.691	0.633
S81021164	16	82.2	0.0012036	344.72	0.926	0.840
S81021968	16	74.6	0.0012028	343.85	0.852	0.772
S81031171	13	53.3	0.0012039	344.43	0.698	0.633
S81031372	13	74.6	0.0011973	344.43	1.183	1.072
S81031373	17	74.6	0.0012011	343.85	0.986	0.894
S81031674	10	65.4	0.0011909	344.43	0.984	0.904
S81032575	14	70.1	0.0012084	343.85	0.996	0.900
S81032676	15	70.0	0.0012104	343.85	1.031	0.928
S81032677	10	48.6	0.0012104	343.85	1.143	1.031
S81032779	12	42.6	0.0012114	343.85	1.163	1.048
S81040881	10	44.1	0.0012104	343.85	1.164	1.049
S81040882	12	53.3	0.0012088	343.85	0.940	0.849
S80141083	9	42.7	0.0012039	343.85	0.945	0.857

Table 3 Wind-tunnel test conditions

M	PT, psia	TT, °F	V, ft/s	$Re\times10^{-6}$, ft^{-1}	$Re_{\bar{c}}\times10^{-6}$
0.30[a,b,d]	1112	89	342	1.0	0.6
0.30[a,c]	2966	123	354	2.5	1.6
0.60[a-d]	641	99	671	1.0	0.6
0.60[a,c]	1608	103	674	2.5	1.6
0.80[a,b,d]	723	84	861	1.4	0.9
0.90[a]	1289	105	1080	2.5	1.5
0.95[a-d]	823	86	1002	1.7	1.0
0.95[a]	1207	89	1004	2.5	1.6
1.05[a,b,c]	849	88	1089	1.8	1.1
1.05[a]	1201	98	1104	2.5	1.6
1.20[b,d]	983	90	1215	2.1	1.3
1.20[a]	1200	104	1230	2.5	1.6
1.20[a]	2486	117	1245	5.0	3.1
1.30[c]	1200	94	1296	2.5	1.6

Notes:
α - Nominal, −4 to 24 deg
β - Nominal, −10 to 10 deg, static tests only
$\omega\bar{c}/2V$ - 0.029 to 0.010
$\omega b/2V$ - 0.029 to 0.009
$P_b b/2V$ - 1.130 to 0.034
Amplitude of oscillation, ±1 deg

[a]Static test. [b]Pitch damping. [c]Roll damping. [d]Yaw damping.

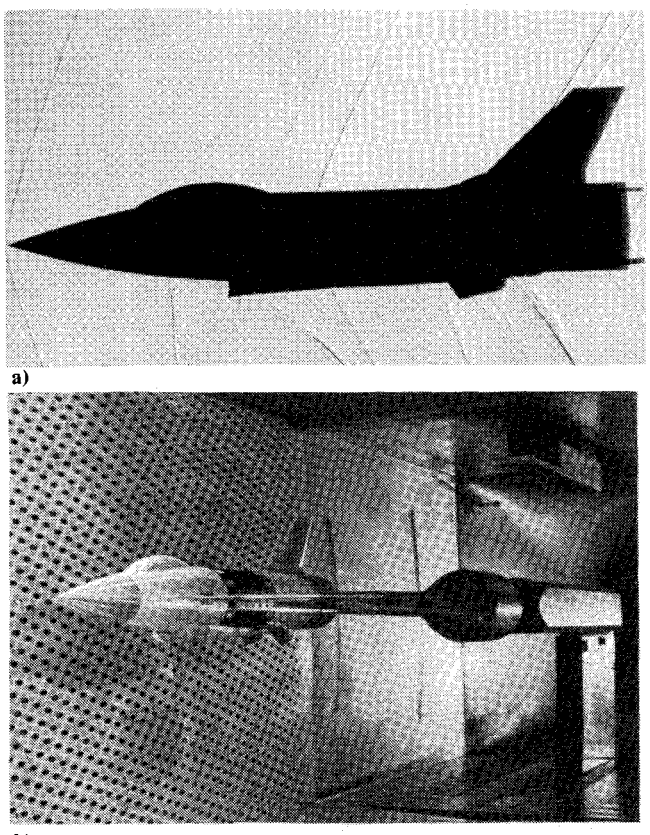

a)

b)

Fig. 3 Model photographs

where $\alpha \approx w_b/V$ and $\beta \approx v_b/V$. The aerodynamic roll angle is computed as follows.

$$\gamma = \tan^{-1}(v_b/w_b) \tag{17}$$

As can be seen, the coefficients are assumed to be functions of Mach number, the sine of the pitch and yaw angles, or the total angle of attack, and the aerodynamic roll angle.

It should be noted that the sine-cosine expansions of the induced terms are ideal and higher order effects have been observed during some wind-tunnel tests at angles of attack greater than 10 deg. However, in the absense of a higher order theory, the ideal model is used.

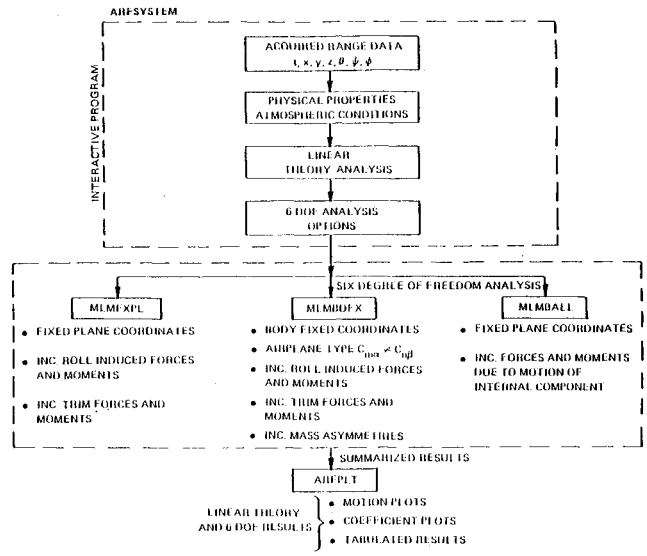

Fig. 4 Data analysis system—aeroballistic research facility

The difference between these aerodynamic expansions and those discussed in Refs. 5 and 6 are the addition of the $C_{x\alpha}$, $C_{z\alpha}$, $C_{m\alpha 2}$, and $C_{l\beta}$ coefficients derivatives. In order to determine the form of the aerodynamic expansions to be included in the free-flight data reduction system, the available wind-tunnel data[3,4] (C_x, C_z, C_y, C_m, C_n, C_l) were fit using polynominals expanded as functions of the components of the angle of attack (α and β). The results of these fits indicated that $C_{x\alpha}$, $C_{z\alpha 2}$, $C_{m\alpha 2}$, and $C_{l\beta}$ terms should be included in the aerodynamic model.

The data reduction methods used to reduce the SDM wind-tunnel data are standard and are presented in Refs. 7 and 8.

Precision of Measurement and Data

Free-Flight Measurements

The precision to which the spatial position and/or orientation of a model can be determined in a ballistic range is generally a principal factor in determining the accuracy of the aerodynamic data extracted from those measurements. The present measuring capability of the ARF is approximately 0.08 deg and 0.03 cm, respectively, for the orientation and position of well-defined points in space.

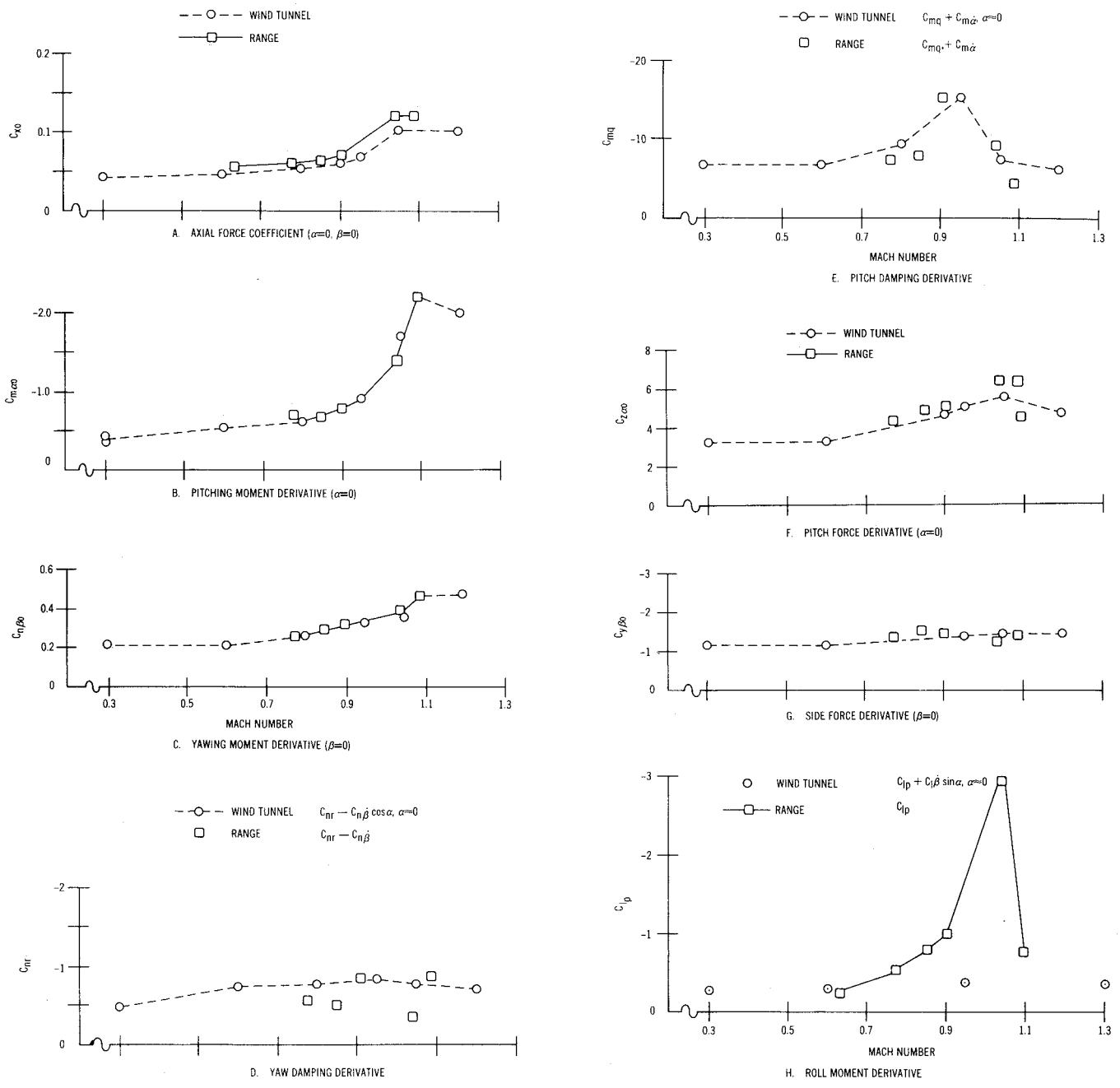

Fig. 5 Comparisons of wind-tunnel and free-flight results.

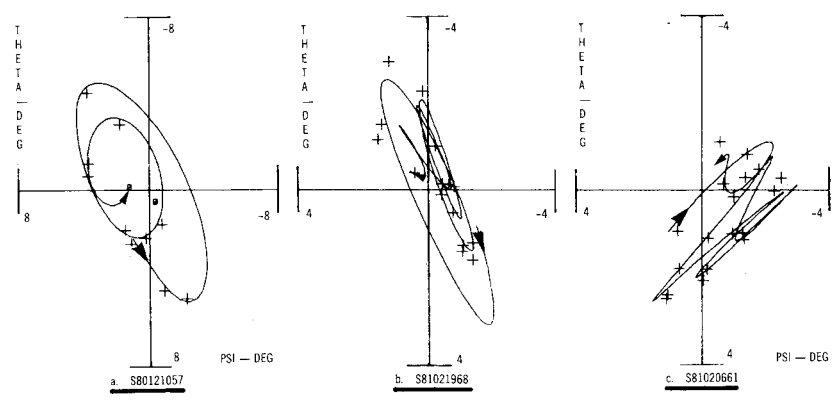

Fig. 6 Typical angular motion profiles (multiple fit $M = 0.775$).

This measurement precision is also related to the geometry of the model. The range coordinates of a model's nose can be determined more precisely if the model has a sharp, well-defined nose tip. Also, the orientation of a long model can be obtained more precisely than that of a short model because the two points (i.e., nose and tail) on the principal axis that defines the orientation are further apart. Therefore, any measurement error associated with the two points has a smaller effect. The SDM is nearly ideal from both aspects and the measurement precisions in orientation and center-of-gravity location are almost identical to the accuracy limits stated earlier.

In addition to facility measurement errors, final aerodynamic data quality is influenced by the quality of the test model and by the applicability of the aerodynamic mathematical model used within the data reduction routines. Both of these error sources were considered in the current tests, and every reasonable effort was made to minimize their effects. Precision constructed models were used in the tests, as noted in the previous section, but because of the complexity of the models and their associated costs in required manhours, some shortcuts were used in the construction process. Therefore, some minor variations in the models were undoubtedly present. These would be expected to effect the quality of the overall multiple fits, and, in turn, the uncertainties associated with the determined aerodynamic coefficients and derivatives. Great care was taken to ensure the applicability of the aerodynamic mathematical model. Additional terms in the coefficient expansions were incorporated, as previously discussed (based on wind-tunnel data), and a multitude of computer runs were accomplished in an attempt to determine if other aerodynamic coefficients were affecting the measured trajectories. For these reasons, it is believed that the mathematical model as modified was adequate for analyzing the present motion profiles.

Wind-Tunnel Data

Measurement uncertainty is a combination of bias and precision errors defined as

$$U = \pm (B + t_{95} S) \tag{18}$$

where B is the bias limit, S the sample standard deviation, and t_{95} the 95th percentile point of the two-tailed Students "t" distribution, which for degrees of freedom greater than 30 equals 2.

The balance data uncertainties were determined from in-place static and dynamic calibrations through the data recording system and data reduction program. Static load hangings on the balance simulate the range of loads and center-of-pressure locations anticipated during the test, and measurement errors are based on differences between applied loads and corresponding values calculated from the balance equations used in the data reduction. Load hangings to verify the balance calibrations are made in-place on the assembled model. Static and dynamic calibrations of the dynamic stability balance system allowed the measurement uncertainty to be that which is due to the amount of nonrepeatability of the calibration constants. The sting and parts of the balance not dynamically calibrated were calibrated by static load hangings over the range of anticipated loads. Uncertainties in the measurements of sting effects were included in the error analysis. Structural damping values were obtained near vacuum conditions before the tunnel flow was started to evaluate the still-air damping contributions.

Propagation of the bias and precision errors of measured data through the calculated data was made, and the detailed results are documented in Refs. 3 and 4. In general, the maximum uncertainty for the wind-tunnel data presented in this paper is within the data symbol.

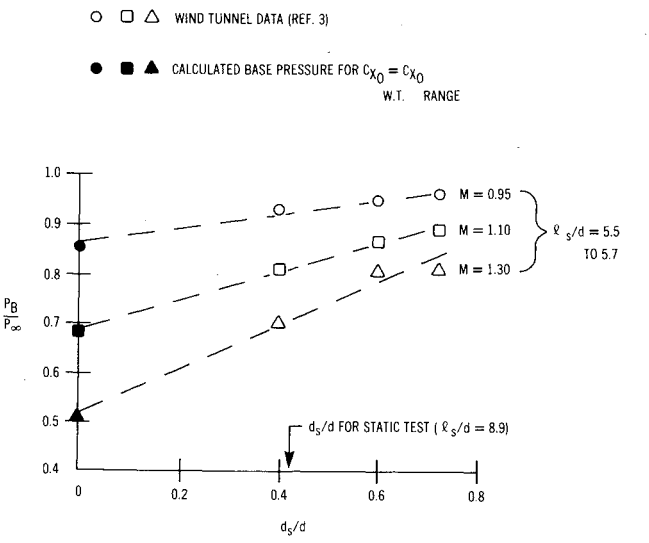

Fig. 7 Base pressure vs sting diam ratio.

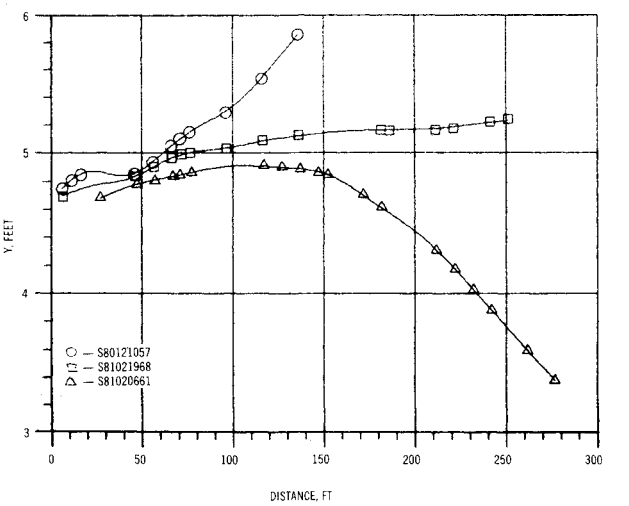

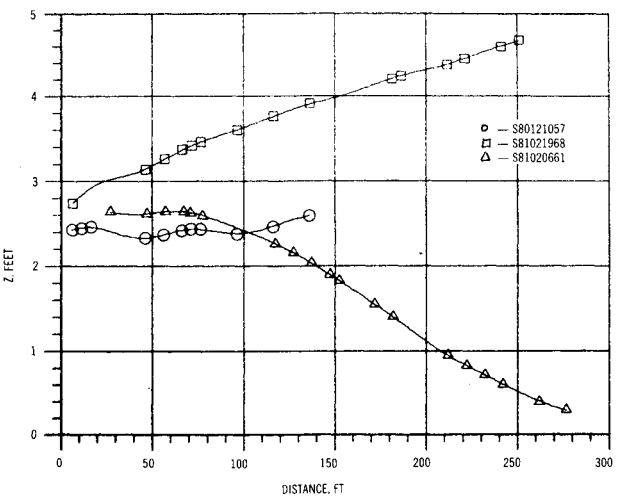

Fig. 8 Typical y and z motions (multiple fit $M = 0.775$).

Results and Discussion

The comparison of the wind-tunnel and free-flight aerodynamic results are shown in Fig. 5. This figure shows a comparison of the zero angle-of-attack coefficients and derivatives, since only relatively small oscillation amplitudes

Table 4 Free flight aerodynamic results (6DOF multiple fit reductions)

Shot No.		Mach No.	DBSQ[a] $\bar{\alpha}_m$ C_{xm}	C_x $C_{x\alpha 2}$ $C_{x\beta 2}$	$C_{y\beta}$ $C_{y\beta 3}$ $C_{y\gamma\alpha 3}$	$C_{z\alpha}$ $C_{z\alpha 3}$ $C_{z\gamma\alpha 3}$	$C_{n\beta}$ $C_{n\beta 3}$ $C_{n\gamma\alpha 3}$	$C_{m\alpha}$ $C_{m\alpha 3}$ $C_{m\gamma\alpha 3}$
S81021063	S81031171	0.630	3.2	0.0553	—	—	—	—
S80121559			4.7	−1.91	—	—	—	—
			0.0	0.0	—	—	—	
S80121057	S81021968	0.775	4.6	0.0600	−1.31	4.08	0.259	−.677
S81020661			5.5	−2.86	0.0	0.0	23.1	0.0
			0.0	0.0	0.0	0.0	−12.9	−10.1
S81020064	S81040882	0.849	3.0	0.0634	−1.52	4.64	0.300	−.657
S81040883			4.1	0.00	0.0	0.0	0.0	0.0
			0.0	0.0	0.0	0.0	−11.6	56.6
S81031674	S81032575	0.908	1.1	0.0701	−1.46	4.83	0.316	−.761
S81032676	S81031373		4.1	−5.54	0.0	0.0	0.0	−123.5
			1.7	0.0	0.0	0.0	51.8	−249.4
S81032677	S81032779	1.044	1.4	0.1170	−1.24	6.20	0.390	−1.36
S81040881			2.5	0.00	0.0	−444.9	0.0	−2076.6
			0.0	0.0	0.0	0.0	45.6	−196.7
S81020560	S81031372	1.092	1.6	0.1174	−1.38	4.33	0.463	−2.18
S80121258			3.9	5.38	0.0	0.0	0.0	−1425.7
			0.0	0.0	0.0	0.0	35.9	−192.5

Shot No.		C_{nr} C_{nr2}	C_{mq} C_{mq2}	$C_{x\alpha}$ $C_{m\alpha 2}$ $C_{z\alpha 2}$	C_{lP} $C_{l\gamma\alpha 2}$ $C_{l\beta}$	PE[b]-X PE[b]-YZ	PE[b]-A PE[b]-R
S81021063	S81031171	—	—	0.000	−0.201	0.0016	—
S80121559		—	—	—	1.656	—	3.461
				—	0.00		
S80121057	S81021968	−0.52	−7.0	0.000	−0.515	0.0011	0.162
S81020661		0.0	0.0	0.0	0.517	0.0009	3.133
				0.0	0.048		
S81020064	S81040882	−0.48	−7.7	0.000	−0.765	0.0013	0.176
S81040883		0.0	0.0	2.2	1.55	0.0015	2.084
				−25.1	−0.01		
S81031674	S81032575	−0.81	−15.1	0.000	−0.765	0.0016	0.142
S81032676	S81031373	0.0	0.0	17.0	2.59	0.0007	1.567
				0.0	0.00		
S81032677	S81032779	−0.33	−9.1	−0.865	−2.93	0.0018	0.150
S81040881		0.0	0.0	−65.4	1.30	0.0014	0.826
				165.0	0.033		
S81020560	S81031372	−0.86	−4.0	0.396	−0.74	0.0010	0.174
S80121258		0.0	0.0	−50.	−0.05	0.0009	1.318
				0.0	0.10		

[a] Effective angle of attack squared. [b] Probable error

were achieved during the free-flight tests (see Fig. 6 for typical angular motion profiles). When viewing the results shown in Fig. 5, it should be remembered that each of the data points representing the determined free-flight aerodynamics were obtained by multiply fitting three or more flights simultaneously. For example, the motions depicted in Fig. 6 were fit to a comon set of aerodynamics which are presented as a single data point in each of the curves of Fig. 5. These flight groupings and the results obtained are shown in Table 4. This table also shows the probable errors associated with the various multiple fits.

The axial force coefficient data shown in Fig. 5a indicates a difference between the levels of the free-flight data and that obtained from the wind tunnel. This might be expected since the presence of a sting could influence the base pressure. Since the sting configuration for the static tests was very similar to the sting used for the pitch-damping tests,[3] the base pressure data obtained during the damping tests were used to construct Fig. 7. The base pressure data are presented as a function of sting diameter ratio. Also shown as solid symbols are the calculated base pressures required for the wind-tunnel axial force to equal the range axial force. The data fairings suggest that the influence of the sting on the base pressure is the reason for the difference in the C_x levels.

The pitching and yawing moment derivatives ($C_{m\alpha 0}$, $C_{n\alpha 0}$) shown in Figs. 5b and 5c, respectively, indicate very good agreement between the wind-tunnel and free-flight measurements. This result is not unexpected since these derivatives are normally determined with very high confidence levels using both the free-flight and wind-tunnel testing techniques (motions are sensitive to these aerodynamic moments). Also, considerable care was taken in matching the

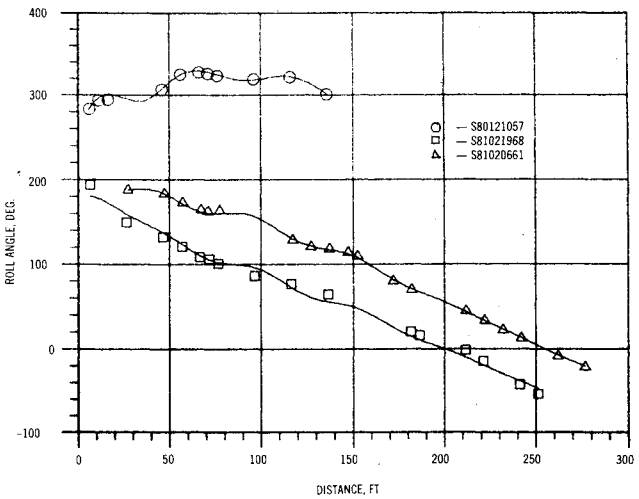

Fig. 9 Typical roll motion (multiple fit $M = 0.775$).

flow conditions (Reynolds number) between the two test facilities.

Although some data scatter is evident in the free-flight damping derivatives (C_{nr} and C_{mq}) as shown in Figs. 5d and 5e, it appears that the general levels and trends are consistent between the two dets of data. The apparent scatter in the free-flight data is most likely caused by the small oscillation angles achieved during the flights. Since these derivatives are a measure of the amplitude decay, the precision to which they can be determined from free-flight trajectories is also a function of the oscillation angles. Even with the free-flight scatter, the agreement between the two sets of data is remarkable considering the drastically different techniques and the inherent difficulty in measuring these derivatives.

The pitch and side force derivatives ($C_{z\alpha}$, $C_{y\beta}$) shown in Figs. 5f and 5g also demonstrate good agreement between the two sets of measurements. Even though the oscillation angles are relatively small for the free-flight tests, the effect these derivatives produced on the measured plunging and swerving motions were significant (see the oscillation in the measured Y and Z curves shown in Fig. 8). Since the $C_{y\beta}$ and $C_{z\alpha}$ derivatives significantly affect the free-flight Y and Z motions, it would be expected that these derivatives could be extracted accurately from the measured motions.

The comparisons of the roll moment derivatives C_{lp} are shown in Fig. 5h. The data appears to agree at the subsonic and supersonic conditions; however, an apparent disagreement exists at the transonic conditions. The free-flight data shows a large increase in C_{lp} near Mach 1, and this is not supported by the wind-tunnel data (see data point at $M = 0.95$). Although an increase in C_{lp} near $M = 1$ would not be unexpected,[9] the magnitude of the increase indicated by the free-flight data is surprising. Even though reasonable fits of the measured free-flight roll motions were achieved (Fig. 9), it is possible that these relatively short flights are not conducive for extracting C_{lp}. There is also the possibility of a modeling or algorithm problem associated with the roll moment derivative in the transonic region. This is not believed to be the case because considerable time and effort was expended incorporating additional terms in the roll moment coefficient expansion and attempting to extract these coefficients using the identification algorithm. None of these efforts reduced the probable errors associated with the roll motion fits or significantly affected the determined C_{lp} values. Therefore, at the present time, it must be concluded that the cause of the discrepancy in the wind-tunnel and free-flight C_{lp} measurements in unknown and warrants further investigation.

Concluding Remarks

A comparison of transonic aerodynamic data obtained from a free-flight spark range and wind tunnel has been successfully completed for the standard dynamics model. Most of these comparisons demonstrate good agreement between the resultant aerodynamic force and moment coefficients. Measurements of the axial force coefficient and the roll moment derivative indicate some differences. The cause of the difference in the axial force coefficient measurements is understood and is discussed; whereas, the cause of the difference in the roll moment derivatives is unknown at the present time. It is believed that the presented comparisons are significant considering the drastically different test facilities and techniques used in obtaining the two sets of data.

References

[1] Winchenbach, G.L. and Chelekis, R.M., "Free Flight Range Tests of the Standard Dynamics Model (SDM) at Transonic Mach Numbers," AFATL-TR-82-5, Dec. 1981.

[2] Winchenbach, G.L., Galanos, D.G., Kleist, J.S., and Lucas, B.F., "Description and Capabilities of the Aeroballistic Research Facility," AFATL-TR-78-14, April 1978.

[3] Cyran, F. B., "Sting Interference Effects on the Static, Dynamics, and Base Pressure Measurements of the Standard Dynamics Model Aircraft at Mach Numbers 0.3 through 1.3," AEDC-TR-81-3, Aug. 1981.

[4] Coulter, S.M. and Marquart, J., "Dynamic Stability Tests of the Standard Dynamics Model Utilizing the New 1500 lb Balance Mechanisms," AEDC-TSR-81-P11, Feb. 1981.

[5] Whyte, R.H., Winchenbach, G.L., and Hathaway, W.H., "Subsonic Free-Flight Data for a Complex Asymmetric Missile," *Journal of Guidance and Control*, Vol. 4, Jan.-Feb. 1981, page 59.

[6] Hatahaway, W.H. and Whyte, R.H., "Aeroballistic Research Facility Free Flight Data Analysis Using the Maximum Likelihood Method," AFATL-TR-79-98, Dec. 1979.

[7] Burt, G.E., "A Description of a Pitch/Yaw Dynamic Stability, Forced Oscillation Test Mechanism for Testing Lifting Configurations," AEDC-TR-73-60, June 1973.

[8] Shuler, C.J., Ward, L.K., and Hodapp, A.E. Jr., "Techniques for Measurements of Dynamic-Stability Derivatives in Ground Test Facilities," AGARDograph 121 (AD669227), Oct. 1967.

[9] West, K.O. and Whyte, R.H., "Free Flight and Wind Tunnel Test of a Missile Configuration at Subsonic and Transonic Mach Numbers with Angles of Attack Up to 30 Degrees," Paper 39, 11th Navy Symposium on Aeroballistics, Trevose, Penn. Aug. 1978.